Journal of Harbin Engineering University Vol 44 No. 11
ISSN: 1006-7043 November 2023

Optimal Location and Sizing of Wind Turbine Generators and Superconducting Magnetic Energy Storage Units in a Distribution System using Grasshopper Optimization Algorithm

Steven Foday Sesay,[1] Cyrus Wabuge Wekesa,[1,2] Livingstone M. H. Ngoo,[1,3]

[1] Department of Electrical Engineering, Pan African University Institute for Basic Science, Technology and Innovation, P.O. Box 62000-00200, Nairobi, Kenya.

[2] School of Engineering, University of Eldoret, Eldoret 1125-30100, Kenya

[3] Department of Electrical Engineering, Multimedia University, P.O. Box 30305, Nairobi, Kenya

Correspondence should be addressed to Steven F. Sesay; foday.steven@students.jkuat.ac.ke

Abstract

Distributed Energy Resources (DERs) are now a common feature in many utilities in the world. In fact, the penetration of power from Wind Turbine Generator (WTGs) into the power distribution system is currently on the rise. However, its variability – combined with variations in load demand- means that there is significant impact on the technical performance of the grid in terms of voltage stability, voltage deviations, and power losses. Superconducting Magnetic Energy Storage (SMES) unit has been shown to be very efficient in addressing these problems because of their fast response, but their high investment cost is a significant barrier. This Paper investigates the performance of a distribution system with embedded WTGs and SMES units through a multi-objective optimization platform to improve technical performance while considering the total cost. Using Voltage Sensitivity Factor (VSF) and the Grasshopper Optimization (GO) algorithm, a weighted sum Multi-objective Function (MOF) is formulated to improve the performance of the distribution system by determining the optimal location and size of WTGs and SMES units, with the weight factors subject to the preference of the decision maker. Simulation tests performed using the proposed algorithm on the IEEE 33-bus distribution system show significant improvement. For example, relative to the base case (no WTGs and SMES units), the following results are found when a WTGs and SMES units are installed: voltage stability shows an improvement of 28.56%; voltage deviation improved by 50.67%; and energy losses were reduced by 29.34%. Results obtained using the GO algorithm were compared with those obtained by equilibrium optimizer (EO) and particle swarm optimization (PSO) algorithms. The numerical results and simulations imply that the employment of WTGs and SMES units can successfully achieve minimization of energy-loss and voltage-deviation as well as enhancement of voltage-stability, and thereby significantly improve the performance of distribution system while considering the total cost.

Keywords: Superconducting Magnetic Energy Storage, Wind Turbine Generator, Distribution System, Voltage Sensitivity Factor and Grasshopper Optimization Algorithm.

1. Introduction

The increasing use of wind energy can be attributed to its significant power generation capacity, reaching up to 10 MW per wind turbine, its cost-effectiveness in terms of kilowatt-hour (kWh) production, and its positive environmental impacts [1]. The annual growth rate of the wind turbine power generation system has experienced a substantial increase in recent years [2]. There are multiple factors that contribute to the global inclination towards the growing utilization of wind turbines for electric power generation. These factors include the escalation of fuel prices, the endorsement of environmentally friendly energy sources, and a significant emphasis on harnessing wind energy. Notwithstanding the advantages associated with wind turbine power generation systems, it is imperative to acknowledge the inherent variability and intermittency of wind energy sources. The proliferation of wind turbine generators in distribution networks presents a range of challenges, such as low voltage stability, voltage deviation, and power loss [3][4]. The incorporation of energy storage systems (ESS) within the distribution system presents a viable approach for addressing these challenges. There are different types of Energy Storage Systems (ESS) employed to address the challenges related to the utilization of WTGs for electric power generation. The aforementioned technologies include battery energy storage system (BESS) [5], flywheel storage [6], fuel cell storage (FC) [7], compressed air energy storage (CAES) [8], compressed carbon dioxide energy storage (CCES) [9], and superconducting magnetic energy storage (SMES) [10].

The BESS exhibits notable limitations, encompassing a short lifespan, limitations in voltage and current, significant environmental implications, and a slow response time, despite its widespread adoption within the industry. In contrast, the SMES unit exhibits several notable advantages. These include a storage efficiency ranging from 95% to 98%, a high power density spanning from 0.1 MW to 10 MW, absence of any mechanical components, swift response time, long lifespan, and unlimited charging and discharging cycles [11]. The installation of

WTGs and SMES units in distribution systems involves significant financial investment. Consequently, it becomes imperative to investigate the performance of a distribution system with embedded WTGs and SMES units through a multi-objective optimization platform to improve technical performance while considering the total cost. The SMES unit has superconducting coil designed to store electrical energy within the magnetic field produced by a direct current (dc) flowing through it [12]. The SMES coil has the capability to either absorb or release real and reactive power, depending on the power requirements of the distribution system. The generation of a magnetic field is facilitated by the dc that passes through the superconducting coil. The energy stored in a SMES unit can be rapidly discharged within a duration of time, spanning from a fraction of a second to several hours [13]–[15]. The main drawback associated with SMES unit is its inflated cost. The aforementioned drawback can be alleviated through the utilization of High Temperature Superconductors (HTS). In contrast to Low-Temperature Superconductors (LTS), High-Temperature Superconductors (HTS) are cooled using liquid Nitrogen to a temperature of 77^{o}K, as opposed to 4.2^{o}K for LTS [14]. The reliability of the HTS system is superior to that of the LTS system, and the associated refrigeration expenses are comparatively lower. A recent review has examined the design and development of high temperature SMES units for power applications [16]. Numerous investigations have been undertaken to explore cooling technologies and thermal management strategies for SMES units, focusing on the utilization of thermal energy storage materials. These efforts aim to alleviate the deterioration in superconductor performance that occurs at elevated temperatures [17]–[22].

Numerous research have been conducted to examine the effectiveness of SMES units in enhancing transient stability [2], [23]–[26], as well as mitigating variations in the output power and voltage of WTGs [27]–[29]. However, there is a scarcity of research regarding the optimal placement and sizing of WTGs and SMES units. The authors in [30] optimally locate an SMES unit in an IEEE14-bus transmission system using a genetic algorithm in order to improve the voltage stability in the test system. In [31], a simplex method was employed to determine the optimal size of the SMES unit to improve the stability of a distribution power system with photovoltaic (PV) generation. The performance of SMES unit with its optimal size is evaluated by a simple case study with the field measurement data of the irradiation and PV module temperature in the Power System Computer Aided Design Software (PSCAD). In [32], the author proposed a method to find the optimal location of the superconducting device for minimizing the system loss using loss sensitivity analysis in an typical power system considering a daily load profile. In [33], the authors proposed a method to minimize the operating cost of thermal units in an IEEE 10-unit thermal transmission system through the use of optimal sized SMES unit using the Lagrange Relaxation PSO algorithm for a daily varying load. Authors in [34] proposed a multi-objective optimization technique for positioning and sizing wind turbine generators and SMES units in a distribution system using the EO algorithm and loss sensitivity factor in an IEEE 33-bus distribution system with time-varying voltage-dependent load models as well as variable wind speed. The weighted sum Multiobjective index was formulated for the simultaneous minimization of energy loss, voltage deviation, and enhancement of voltage stability. It can be deduced that more recent optimization techniques need to be investigated in the location and sizing of WTGs and SMES units.

This work proposes a hybrid VSF and GO algorithm technique for determining the optimal location and sizing of WTGs and SMES units in the IEEE 33-bus distribution system. The efficiency of the GO algorithm is validated by comparing it with the results obtained by the EO and PSO algorithms. Currently, there is no documentation on the utilization of the hybrid VSF-GO algorithm technique for locating and sizing WTGs and SMES units. The location and sizing of WTGs and SMES units have utilized four objective indices: voltage stability index, voltage deviation index, power loss index , and annual total cost.

2. Methodology

This section describes the materials and methods used in this research.

2.1. Network Component Modeling.

The model under study consists of the IEEE 33-bus distribution system and load demand profile, WTGs and SMES units.

2.1.1. IEEE 33-Bus Distribution System and Load Demand Profile

The test bus system is a modified IEEE 33-bus radial distribution system as shown in Figure 2. It consists of thirty-three buses and thirty-two lines (branches). All buses have a voltage level of 12.66 kV. The maximum and minimum voltage limits for all buses are considered at ±5%. The network can be fed either by a synchronous generator or from the main grid. The basic data of the IEEE 33-bus distribution system is shown in Table 1 [35].

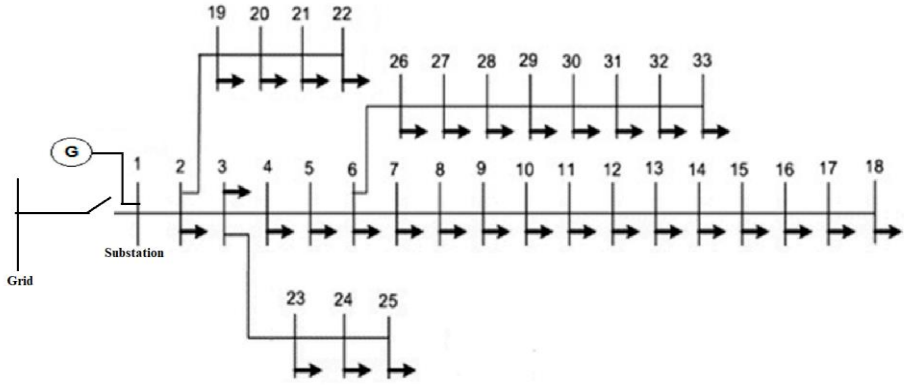

FIGURE 2: Single line diagram for the IEEE 33-bus distribution system [35]

The normalized hourly load demand profile of 1 p.u peak [34] is considered in the study as shown in Figure 3. The loads are of time-varying voltage-dependent type with active load-voltage exponent (n_p) of 4.04 and reactive load-voltage exponent (n_q) of 0.92 [36].

TABLE 1: Basic data of IEEE 33-bus distribution system [35]

Parameters	Values
Base Voltage (kV)	12.66
Nominal Active Load (kW)	3715
Nominal Reactive Load (Kvar)	2300
Base MVA	100

The time-varying voltage-dependent load model at bus k of the distribution network is expressed in equations (1) and (2):

$$P_k(t) = P_{ok}(t)x\, V_k^{np}(t) \quad (1)$$

$$Q_k(t) = Q_{ok}(t)x\, V_k^{nq}(t) \quad (2)$$

where P_k and Q_k are, respectively, the real and reactive powers injected at the k^{th} bus, P_{ok} and Q_{ok} are, respectively, the real and reactive loads at the same bus but at nominal bus voltage, V_k is the voltage at the bus for n_p and n_q respectively.

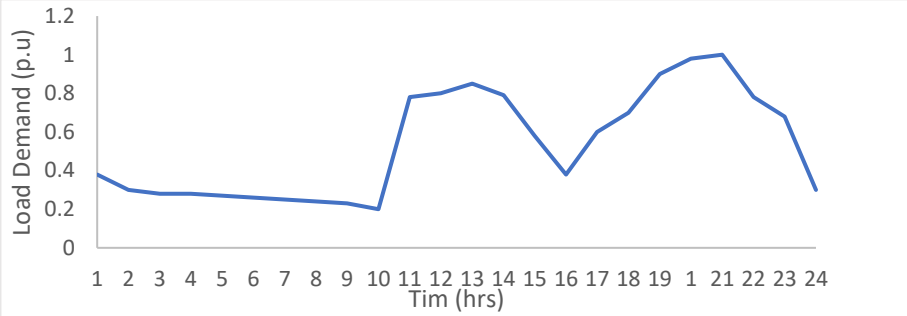

FIGURE 3: Normalized hourly load demand profile [36]

2.1.2. WTG Modeling

The WTG generated outpower P_{WTG} at wind speed v_w is determined as shown in equation (3).

$$P_{WTG} = \begin{cases} 0 & \text{if } V_w \langle V_{ci} \text{ and } V_w \rangle V_{co} \\ \left\{p_{w,r}\left(\frac{V_w - V_{ci}}{V_{w,r} - V_{ci}}\right)\right\} & \text{if } (V_{ci} \le V_w \le V_{w,r}) \\ P_{w,r} & \text{if } (V_{w,r} < V_w \le V_{co}) \end{cases} \quad (3)$$

where $P_{w,r}$ is the rated output power and V_{ci},V_{co}, and $V_{w,r}$ are the cut-in speed, cut-out speed, and rated speed of the WTG, respectively. Equation (3), which represents the WTG characteristic power curve, demonstrates that there is no WTG output power when the wind speed is lower or higher than the cut-in and cut-out wind speeds, respectively. It also demonstrates a constant rated output power for wind speed between the rated and cut-out wind speeds, as well as a linear relationship when the wind speed varies between the cut-in and the rated wind speed [37]. The wind speed $v_w(h)$ at WTG hub-height (h) determines the amount of power P_{WTG} that the wind turbine generates, and this wind speed is stated as shown in equation (4):

$$v_w(h) = v_w(h_g)x\left(\frac{h}{h_g}\right)^{\alpha} \quad (4)$$

where $v_w h_g$ is the anemometer-measured wind speed at height h_g and is a roughness factor that varies from site to site and depends on the local humidity, but several studies suggest a value of 1/7 [38].

The ratio of the total energy supplied by the WTG to the total energy required by the system is known as

the WTG penetration level. The technical specifications of the three (3) WTGs used in the study are shown in Table 2. The 3.3 MW rated output power is used when one WTG is considered and the 1.7 MW rated output power is considered when two (2) WTGs are considered. The hourly wind speed curve is shown in Figure 4 [35].

$$\text{WTG penetration (\%)} = \frac{\sum_{t=1}^{24} P_{WT}(t)}{\sum_{t=1}^{24} P_L(t)} \quad (5)$$

TABLE 2: Technical specifications of wind turbine generators [39]

Parameters	WTG-1	WTG-2	WTG-3
Cut-in speed (m/s)	4	4	4
Rated speed (m/s)	14	14	14
Cut-out speed (m/s)	24	24	24
Rated output power (MW)	3.3	1.7	1.1

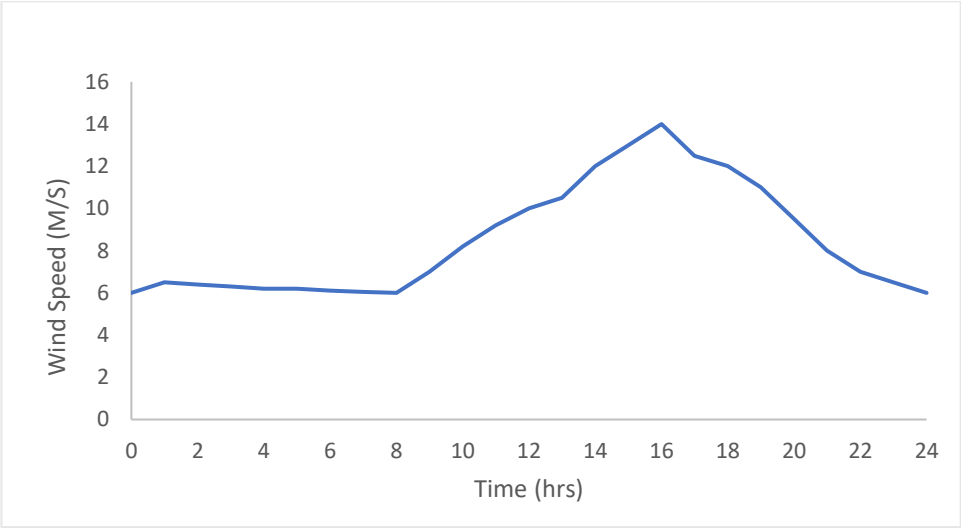

FIGURE 4: Hourly wind speed curve [35]

2.1.3. SMES Unit Modeling

The SMES unit can store the surplus or excess energy generated by the WTG rather than curtailing it when the load demand is low and release energy to supply the peak load demand during the day. Expressly, the SMES unit can operate as loads to store energy during charging mode and generators to release load or deliver energy during discharge mode. The SMES unit is allowed to discharge when wind turbine generator outpower is low and the load is larger than 75% of the peak load demand. It can deliver or absorb reactive power as well. To charge the SMES unit from WTG, they are installed on the same bus as the WTG.

Charging mode:

This mode occurs when WTG power P_{WTG} is higher than the load demand P_L (i.e., $P_L - P_{WTG} < 0$ or $P_s(t) < 0$).

$$P_s(t) = \max\left\{-|\Delta p(t)|, \frac{(E_S(t-1)-E_{S,max})}{\Delta t \eta_c}\right\}, -P_{s,rated} \quad (6)$$

$$E_s(t) = \min\{(E_s(t-1) - P_{s,c}(t)\Delta t \eta_c), E_{s,max}\} \quad (7)$$

Discharge mode:

This mode occurs when the load demand P_L is higher than the WTG power P_{WTG} (i.e., $P_L - P_{WTG} > 0$ or $P_S(t) > 0$).

$$P_S(t) = \max\left\{|\Delta p(t)|, \frac{(E_S(t-1)-E_{S,max})}{\Delta t \eta_c}\right\} \quad (8)$$

$$E_S(t) = \max\left\{\left(E_S(t-1) - P_{S,D}(t)\frac{\Delta t}{\eta_D}\right), E_{S,min}\right\} \quad (9)$$

Where $P_S(t)$ is the exchanged power of the SMES unit at period t, which has negative, positive, and equal to zero during charging mode, discharging mode, and idle mode of the SMES unit respectively and where η_C and η_D are the charging and discharging efficiencies, respectively; The difference between load demand and WTG output is known as $\Delta P(t)$; $P_{S,rated}$ denotes the power rating of the SMES unit ; $E_s(t)$ denotes its energy storage capacity at period t; $E_{S,min}$ and $E_{s,max}$ denote the minimum and maximum energy storage capacity limits of the SMES unit respectively; and Δt represents the time interval (one hour) [5], [33], [40], [41].

2.2. Location and Sizing

The problem is to optimally locate and size WTGs and SMES units in the test distribution system using

VSF and the GO algorithm. The study considers three cases: Case I (one WTG and one SMES unit), Case II (two WTGs and two SMES units), and Case III (three WTGs and three SMES units).

2.2.1. Voltage Sensitivity Factor

Voltage sensitivity studies are conducted to determine the connection between bus voltage and active or reactive power. In the distribution system, the relationship between voltage magnitude and active or reactive power is not as in the transmission system because low and medium-voltage conductors have a large resistance component. Therefore, the system needs both active and reactive power supply. Therefore, the voltage sensitivity factor plays a crucial role in the location and size of WTGs and SMES units due to the combined effect of active and reactive power on bus voltage. In this study, four indices derived from Newton-Raphson power flow calculation are used for evaluating the sensitivity of active and reactive (PQ) nodes in the distribution system [42] as shown in equations (10)-(13).

$$\text{Index}_{1_i} = \frac{\sum_{k=1}^{n} \frac{\partial \delta_i}{\partial P_i}}{n} \quad (10)$$

$$\text{Index}_{2_i} = \frac{\sum_{k=1}^{n} \frac{\partial |V_i|}{\partial P_i}}{n} \quad (11)$$

$$\text{Index}_{3_i} = \frac{\sum_{k=1}^{n} \frac{\partial \delta_i}{\partial Q_i}}{n} \quad (12)$$

$$\text{Index}_{4_i} = \frac{\sum_{k=1}^{n} \frac{\partial |V_i|}{\partial Q_i}}{n} \quad (13)$$

The flow chart of the methodology is depicted in Figure 5. The steady state planning methodology calculates the indices once the Newton-Raphson method converges to meet the requirements of the power flow. A change in the loading condition is applied at a selected node in the distribution system and the indices are recalculated. After following this procedure for various loading conditions, the voltage sensitivity indices for each node are obtained. The buses with low VSF are selected as the candidate bus for installing WTGs and SMES units.

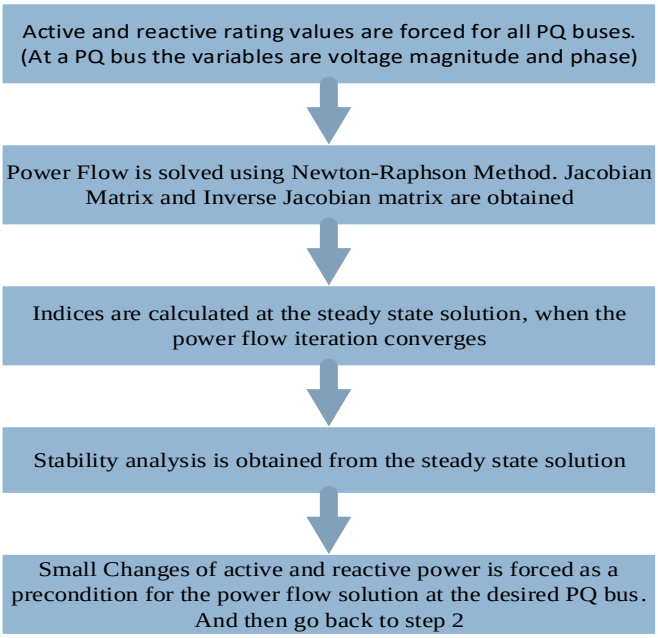

FIGURE 5: Diagram of the process used to calculate the indices.

2.3. Problem Formulation

The optimization problem for the optimal location and sizing of WTGs and SMES units is formulated as a weighted sum multi-objective function for enhancement of voltage stability, minimization of voltage deviations, power loss and annual total cost. Mathematically, this multiobjective function can be stated as shown in equation (14).

$$\text{Minimize } F(\vec{X}) = \left(\frac{1}{F_1(\vec{x})}, F_2(\vec{x}), F_3(\vec{x}), F_4(\vec{x})\right) \quad (14)$$

$$\text{w.r.t } (\vec{x}) = \left[\vec{L}_{WTG}, \vec{S}_{WTG}, \vec{L}_{SMES}, \vec{S}_{SMES}\right]$$

$$\text{Subject to } \begin{bmatrix} H_n = 0, n = 1,2 \ldots \ldots q \\ Yn \geq 0, n = 1,2, \ldots . . p \end{bmatrix}$$

Where $(\vec{x})$ is a vector of control variables that will be optimized in the process. L_{WTG}, and L_{SMES} are the vectors denoting the location of the WTGs and SMESs, respectively. S_{WTG} and S_{SMES} are the vectors denoting the capacities (sizes) of the WTGs and SMES units, respectively. The terms H_n and Y_n denote the equality and inequality constraints to

account for the technical restrictions and operating strategies, respectively. Note that the control variables include both integer and positive real values. The impact indices and the equality and inequality constraints are presented in the following subsections.

2.3.1. Impact Indices

The distribution system before the insertion of WTGs and SMES units is referred to as "base case" throughout this work.

2.3.1.1. Voltage Stability Index

The first objective function F_1 is defined as the Voltage Stability Index (VSI) for the base case value and after insertion of WTGs and SMES units as shown in equation (15) [43].

$$F_1 = \frac{\sum_{i=1}^{nb} |VSI_{(k)}|_{(\text{base case})}}{\sum_{i=1}^{nb} |VSI_{(k)}|_{(WTG,SMES)}} \quad (15)$$

The VSI is determined as follows:

$$VSI_{(k)} = |V_i|^4 - 4(P_k X_{ik} - Q_k R_{ik})^2 - 4(P_k X_{ik} + Q_k R_{ik})|V_i|^2 \quad (16)$$

Where $VSI_{(k)}$ is the voltage stability index at bus k and X_{ik} is the line reactance between i and k buses.

2.3.1.2. Voltage Deviation Index

The second objective function F_2 is defined as the voltage deviation from the rated value after insertion of WTGs and SMES units referring to as its value for the base case as shown in equation (17).

$$F_2 = \frac{\sum_{i=1}^{nb} |V_i - V_{ref}|_{(WTG,SMES)}}{\sum_{i=1}^{nb} |V_i - V_{ref}|_{(\text{base case})}} \quad (17)$$

Where n_b is number of buses, V_i is the voltage at bus i, and V_{ref} is the reference voltage being equal to 1 p.u.

2.3.1.3. Active Power Loss Index

The third objective function F_3 is defined as the active power loss after insertion of WTGs and SMES units refers to as its value for the base case as shown in equation (18).

$$F_3 = \frac{\sum_{\ell=1}^{n\ell} P_{Loss(WTG,SMES)}}{\sum_{\ell=1}^{n\ell} P_{Loss(\text{base case})}} \quad (18)$$

Where $n\ell$ is number of transmission lines in the investigated distribution system.

2.3.1.4. Annual Total Cost

The annual total cost comprises of the annual investment, operation, and maintenance costs. The costs of the WTGs and SMES units are influenced by the market economy and the site location of the installation. While the cost of SMES units is influenced by both its power and energy ratings, the cost of WTG is determined by its power rating. Therefore, it is preferable to express the cost of WTGs and SMES units separately [44], [45]. Its objective function is expressed in equations (19) through (23). The annual total cost in Million US Dollars (MUSD) is obtained when considering the minimum sizes of WTGs and SMES units and is represented as Cost (WTGs, SMESs), and the maximum annual total cost of (WTGs and SMESs) in MUSD is obtained when considering the maximum capacities and is represented as $\text{Cost (WTG, SMES)}_{max}$ as shown in equation (19).

$$F_4 = \frac{\sum_{i=1}^{nb} \text{Cost(WTG,SMES)}}{\sum_{i=1}^{nb} \text{Cost (WTG,SMES)}_{max}} \quad (19)$$

$$\text{Annual total cost} = C_{WTG} + C_{SMES-E} + C_{SMES-P} \quad (20)$$

Where,

$$C_{WTG} = \sum_{n=1}^{N_{WTG}} \left(\overline{IC}_{WTG} x\, C_{\lambda_{WTG}} + \overline{0\&M}_{WTG}\right) x\, S_{WTG} \quad (21)$$

$$C_{SMES-E} = \sum_{n=1}^{N_{SMES}} \left(\overline{IC}_{SMES-E} x\, C_{\lambda_{SMES-E}} + \overline{0\&M}_{SV}\right) x\, E_{SMES} \quad (22)$$

$$C_{SMES-P} = \sum_{n=1}^{N_{SMES}} \left(\overline{IC}_{SMES-P} x\, C_{\lambda_{SMES-P}} + \overline{0\&M}_{Sf}\right) x\, P_{SMES} \quad (23)$$

$\overline{IC}$ denotes the unit investment cost of WTGs and SMES units in USD/kW or USD/kWh, whereas $(\overline{O\&M})$ denotes the annual operation and maintenance costs of the units in USD/kW-yr or USD/kWh-yr. It should be noted that λ is the estimated lifetime of the units in years, S_{WTG} is the size of installed SMES unit; E_{SMES} and P_{SMES} represents the energy and power rating of the SMES units. The subscripts f and v in $(\overline{O\&M})$ denote the fixed and the variable operation and maintenance costs of SMES units respectively. The number of WTGs and SMES units are represented by N_{WTG} and N_{SMES}, respectively. Finally, C_λ is the capacity recovery factor of a unit having a lifetime of C_{λ_x}, with an interest rate of r. The WTGs and SMES units' parameters are shown in Table 3.

TABLE 3: WTGs and SMES units cost parameters [3], [46][44]

Maximum N_{WTG} = 1, 2 and 3 Maximum NSMES =1, 2 and 3	$\overline{IC}_{WTG}$(MUSD\$/kW) = 0.00025-0.0005	$\overline{IC}_{SMES}$(MUSD\$/kWh) = 0.0005
λ_{WTG}(year)= 25	$\overline{O\&M}_{WTG}$ (MUSD\$/kW-yr): 0.08 - 0.25	$\overline{O\&M}_{SV}$ (MUSD\$/kW-yr): $1x10^{-10}$
P_{SMES} (MUSD\$/kW)= 0.0002	λ_{SMES} = 30	$\overline{O\&M}_{Sf}$ (MUSD\$/kW-yr): 0.0000185

Maximum WTGs rated power limit: 0.4 - 4.0 MW	E_{SMES} (MUSD$/kWh)= 0.0005	$\overline{IC}_{SMES}$(MUSD$/kW) = 0.00025
SMES units rated power limit : 0.01- 4.0 MW	SMES units rated capacity limit: 0.001- 10.0 MWh	

2.3.2. Weighted-Sum Multi-Objective Index

A weighted sum multiobjective index (MOI) is formulated to accommodate the above indices with appropriate weights as shown in equation (24).

$$MOI(t) = \mu_1 F_1 + \mu_2 F_2 + \mu_3 F_3 + \mu_4 F_4 \quad (24)$$

Where μ_1, μ_2, μ_3 and μ_4 denote weight factors, each weight factor has the range from zero to one and whose summation is equal to one as shown in equation (25).

$$|\mu_1| + |\mu_2| + |\mu_3| + |\mu_4| = 1 \quad (25)$$

The determination of MOI(t) at each hour is performed using load flow analysis of the distribution system. The Average Multiobjective Function (AMOF) over the total day hours (T=24) is expressed as shown in equation (26)

$$AMOF = \frac{1}{T}\int_0^T MOI(t) \times \Delta t \quad (26)$$

The lowest AMOF value identifies the best sizes of WTGs and SMES units for enhancing voltage stability, minimizing voltage deviation and power loss while considering the total cost.

2.3.2.1. Weight Factors

The weight factors are left to the discretion of the decision maker. In this work μ_1,μ_2, μ_3 and μ_4 are 0.3,0.4,0.2 and 0.1 as it has a consistent impact on the voltage stability index and voltage deviation.

2.3.3. Problem Constraints

The AMOF expressed in (26) is subjected to the following constraints:

2.3.3.1. System Operation Constraints

i. Power balance constraint

The algebraic sum of all input and output active and reactive power flow through the investigated distribution system should be equal as shown in equations (27) and (28)

$$P_{sub}(t) + \sum_{i=1}^{nb} P_{WTG,i}(t) + \sum_{i=1}^{nb} P_{S,i}(t) = \sum_{\ell=1}^{n\ell} P_{loss,\ell}(t) + \sum_{i=1}^{nb} P_{L,i}(t) \quad (27)$$

$$Q_{sub}(t) = \sum_{\ell=1}^{n\ell} Q_{loss,\ell}(t) + \sum_{i=1}^{nb} Q_{L,i}(t) \quad (28)$$

where $P_{Sub}(t)$ and $Q_{Sub}(t)$ represents substation active and reactive power at time t, respectively, $P_{loss}\ell(t)$ and $P_{loss}\ell(t)$ are active and reactive power losses of line ℓ at time t, $P_{L,i}(t)$ and $Q_{L,i}(t)$ are active and reactive powers of load demand at bus i at time t [47].

ii. Bus Voltage Constraint

The voltage magnitude at each bus must be kept within an acceptable range at all times as shown in equation (29).

$$V_{min} \le V_i(t) \le V_{max} \quad (29)$$

Where V_{min} and V_{max} are the minimum and the maximum voltage limits with values of 0.95 p.u. and 1.05 p.u., respectively.

iii. Line current constraint

The current magnitude of each line I_ℓ at any time t must remain within acceptable operating limits in order to avoid any excessive thermal stress of the line is shown in equation (30).

$$I_\ell(t) \le I_{max,\ell} \quad (30)$$

iv. Reverse Power Flow Constraint

This constraint defines that the reverse power flow never exceeds 0.6 of the substation rating (R) is shown in equation (31) [47].

$$-0.6XR \le P_{sub}(t) \le R \quad (31)$$

2.3.3.2. Wind Turbine Constraints

The wind turbine constraint is shown in equation (32).

$$P_{WTG,min} \le \sum_{i=1}^{nb} P_{WTG,r,i} \le P_{WTG,max} \quad (32)$$

Where $P_{WTG,min}$ is equal to 0 and $P_{WTG,max}$ is equal to maximum rated output power of the WTG.

2.3.3.3. SMES Unit Constraints

The charging-discharging power limit constraint is shown in equation (33).

$$-p_{S,rated} \le P_s(t) + P_{S,rated} \quad (33)$$

Where the negative and positive polarities of $p_{S,rated}$ refers to charging and discharging of SMES units, respectively.

2.3.3.4. Storage Capacity Constraint

The storage capacity constraint is shown in equation (34).

$$E_{S,min} \le E_S(t) \le E_{S,max} \quad (34)$$

where $E_{S,min}$ and $E_{S,max}$ are taken as 0.1 and 0.9 times rated capacity $E_{S,rated}$ respectively [1], [33], [48].

2.3.3.5. Capacity Balance Constraint

For continuous utilization in the next day, the final storage capacity $E_s(t)$ of SMES unit at the end of the day should be equal to the initial storage capacity $E_s(0)$ for the next day as shown in equation (35).

$$E_s(0) = E_s(t) \quad (35)$$

2.4. Grasshopper Optimization Algorithms

The metaheuristic algorithms have the capability to give various solutions, which can be evaluated for the best outcome depending on the system constraints. That is the reason it is preferred over mathematical algorithms that result in only one solution, while more than one solution may be available [49]. It is known from the No Free Lunch theory [50] that no optimization algorithm can solve all types of optimization problems. In this work, the GO algorithm is investigated for the optimal location and sizing of WTGs and SMES units in a distribution system.

Saremi et al. introduced the GO algorithm in [51], which is a new and fascinating swarm intelligence system that mimics grasshopper foraging and swarming behaviors. Grasshoppers are insects that wreak havoc on agricultural products. Their life cycle includes two phases: nymph and adulthood. Small steps and gradual movements describe the nymph phase, but long-range and abrupt movements represent the adulthood phase. The intensification and diversification phases of GO algorithm are defined by nymph and adult movements. The mathematical model of grasshopper swarming behavior is shown in equation (36)

$$P_i = S_i + G_i + A_i \quad (36)$$

where P_i indicates the i-th grasshopper's position, S_i is the social interaction between grasshoppers, G_i denotes the gravity force on the i-th grasshopper, and A_i is the wind advection. To produce a random behavior of grasshoppers, equation (37) can be rewritten as follows:

$$P_i = r_1 S_i + r_2 G_i + r_3 A_i \quad (37)$$

Where r_1, r_2 and r_3 are random numbers in the range [0,1]

The social interaction S_i is defined in equation (38)

$$S_i = \sum_{\substack{j=1 \\ j\neq i}}^{N} s(d_{ij})\widehat{d_{ij}} \quad (38)$$

Where N denotes the number of grasshoppers, $d_{ij} = |P_j - P_i|$ defines the Euclidean distance between the i-th and the j-th grasshopper is a unit vector from the i-th to the j-th grasshopper, $\widehat{d_{ij}} = \frac{P_j - P_i}{d_{ij}}$ and s represents the social forces represented by equation (39)

$$S(r) = f\exp^{\frac{-r}{l}} - \exp^{-r} \quad (39)$$

Where f and l are the attraction intensity and attraction length scale, respectively. The social interaction between grasshoppers can be defined as attraction and repulsion. The distance is considered in the range [0,15]. The attraction increases in the interval of [2.079, 4] and then decreases gradually. The repulsion occurs in the range [0, 2.079]. When the distance between two grasshoppers is exactly 2.079, there is neither repulsion nor attraction (no force). This area is called the comfort zone.

The gravity force G_i is given by the equation (40)

$$G_i = -g\widehat{e_g} \quad (40)$$

Where g denotes the gravitational constant and $\widehat{e_g}$ represents a unit vector toward the center of earth.

The wind advection A_i is given by the equation (41):

$$A_i = u\widehat{e_w} \quad (41)$$

Where u represents the drift constant and $\widehat{e_w}$ is a unit vector in the wind direction.

After replacing the values of S, G, and A, equation (42) can be obtained:

$$P_i = \sum_{\substack{j=1 \\ j\neq i}}^{N} s(|P_j - P_i|)\frac{P_j - P_i}{d_{ij}} - g\widehat{e_g} + u\widehat{e_w} \quad (42)$$

An enhanced version of this equation is shown in equation (43)

$$P_i^d = C\left(\sum_{\substack{j=1 \\ J\neq i}}^{N} c\frac{u_{bd} - l_{bd}}{2} s(|p_j^d - p_i^d|)\frac{p_j - p_i}{d_{ij}}\right) + \widehat{T_d} \quad (43)$$

Where u_{bd} and l_{bd} represent the upper and lower bounds in the d-th dimension, respectively. $\widehat{T_d}$ denotes the best solution found so far in the d-th dimension space. Note that S is similar to S component in equation (38), G is equal to zero, and A is always toward the best solution $\widehat{T_d}$. Equation (44) is used to calculate the value of C.

$$C = C_{max} - t\frac{C_{max} - C_{min}}{t_{max}} \quad (44)$$

The step procedure for the GO algorithm is listed as follows [52][53]:

Step 1: Input system data including line data, bus data, and wind speed data.

Step 2: Input design variables in the problem as well as the parameters of GO algorithm.

Step 3: Initialize randomly the particle's population.

Step 4: Estimate the objective function of each initial solution.

Step 5: Update C

Step 6: Normalize the distance between Grasshoppers in the range [1-4]

Step 7: Evaluate the objective function.

Step 8: Check the convergence criteria. The algorithm terminates when the number of iterations exceeds the limits T_{max}, or a satisfactory fitness level has been reached for the population with satisfaction of the problem constraint.

Step 9: Capture the optimal solution (best objective function) to the target problem.

3. Results and Discussions

This section presents the results obtained for optimal location and sizing of WTGs and SMES units using VSF and GO algorithms for improving the technical performance of the IEEE 33-bus distribution system while considering the total cost. The simulation is carried out on an HP personal computer with an Intel Core (TM) i7, 16 GB of RAM, and a 64-bit operating system using the MATLAB R2020b software package. Forward/backward flow analysis is performed without WTGs and SMES units for the base case and with WTGs and SMES units for cases I, II, and III in the IEEE 33-bus distribution system. The optimal location and sizing of WTGs and SMES units is performed considering three different cases: firstly, the installation of one WTG and one SMES unit. Secondly, the installation of two WTGs and two SMES units, and thirdly, the installation of three WTGs and three SMES units. Finally, the effectiveness of the proposed algorithm is validated by comparing it with EO and PSO in terms of statistical metrics and convergence time. In this work, the simulation is performed, and the results are recorded and analysis to obtain the tables and figures. Table 5 shows the load flow results obtained for the IEEE 33-bus distribution system without considering the load demand profile. P_s is the active power supply (MW), P_L is the active load demand, $VSI_{(basecase)}$ is the voltage stability index at the base case, $VDI_{(base\ case)}$ is the voltage deviation index at the base case, and $P_{loss\ (basecase)}$ is the active power loss at the base case.

TABLE 5: Base case data

P_s (kW)	P_L (kW)	$VSI_{(basecase)}$	$VDI_{(base\ case)}$	$P_{loss\ (basecase)}$ (kW)
3716	3715	0.7326	0.8925	0.2021

3.1. Optimal Location and Sizing Selection

The WTGs and SMES units are optimally located and sized using hybrid VSF and GO algorithm techniques. The optimal location and sizing result for cases I, II, and III are shown in Table 6. It was deduced that as the number of installed WTGs and SMES units are increasing and optimal placed in the distribution system, the technical performance of the distribution system improves, which needs to be balanced with the cost f of the WTGs and SMES units.

TABLE 6: Optimal location and sizing results for cases I, II, and III

Items	Case I	Case II	Case III
WTGs location and Size (kW/@ Bus)	3831/@ 18	2132 /@ 28 1699/@ 21	930/@ 28 1553/@ 17 1448/@ 21
SMES Sizes (kW/kWh)	2200/9094	1100/4738 1100/4356	610/3100 860/2830 753/2480
AMOF value	0.2831	0.2609	0.2509
VSI enhancement (%)	28.56	29.43	30.14
VDI reduction (%)	50.67	52.59	54.68
Energy Loss reduction (%)	29.34	37.76	41.56

Furthermore, the value of the AMOF of the complete day for the time-varying load decreases as the number of WTGs and SMES units increases in the test distribution system which has a base case AMOF value of unity.

3.1.1. Voltage Stability Analysis

The Voltage Stability Index (VSI) is an indication of distribution system stability. It is driven based on the magnitudes of the voltage and current of the system in order to obtain the distance between the operating point of the current and the collapse point of the voltage. The smaller the value, the more sensitive the system is to voltage collapse. In the distribution system, the voltage stability is computed as the algebraic sum of all hourly voltage stability over the day. Table 7 shows a comparison of the daily voltage stability of the system for the base case and after installation of the WTGs and SMES units for cases I, II, and III. It is clearly observed that the voltage stability enhancement in the distribution system for cases I, II, and III are 28.56%, 29.43%, and 30.14%, respectively.

TABLE 7: Voltage stability index for cases I, II and III

Case	Daily voltage stability Index		Voltage stability improvement (%)
	Base case	After	

One WTG and One SMES (I)	691.38	493.86	28.56
Two WTGs and Two SMESs (II)	691.38	487.91	29.43
Three WTGs and Three SMES (III)	691.38	483.00	30.14

The hourly values after installation of WTGs and SMES units are higher than those of the base case and for cases I, II, and III, as illustrated in Figure 7. This value approaches unity to express the best voltage stability of the distribution system. It was deduced that as the number of installed WTGs and SMES units increases, the VSI value approaches unity, which is the best voltage stability index value.

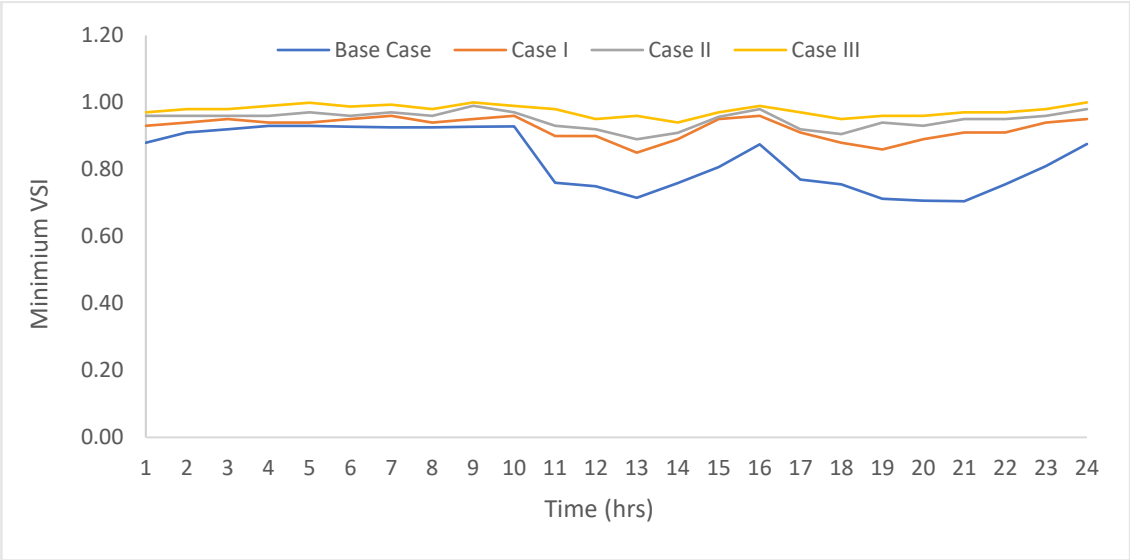

FIGURE 7: Hourly minimum VSI for the cases

3.1.2. Voltage Deviation Index

The Voltage Deviation Index (VDI) of a node in the distribution system is the difference between the actual voltage of the node and the reference voltage (1 p.u). The lower the value, the more stable is the voltage of the system. The voltage is computed as the algebraic sum of all hourly voltage deviations over the day. Table 8 shows the comparison of the daily voltage deviation of the system for the base case and after installation of WTGs and SMES units for cases I, II, and III. It was observed that the voltage deviation indices of the distribution system for cases I, II, and III were significantly reduced compared to their base cases. The voltage deviation reduction in the distribution system for cases I, II, and III are 50.67%, 52.59%, and 54.68%, respectively. As illustrated in Figure 8, the hourly minimum bus voltage (the weakest bus # 18) over the day hours after installation of WTGs and SMES units for the study cases is significantly improved compared with that of the base case of the system and are within the permissible limit during the day hours.

TABLE 8: Voltage deviation for cases I, II and III

Case	Daily voltage deviation		Voltage deviation reduction (%)
	Base Case	After	
One WTG and One SMES (I)	19.49	9.61	50.67
Two WTGs and Two SMESs (II)	19.49	9.24	52.59
Three WTGs and Three SMES (III)	19.49	8.82	54.68

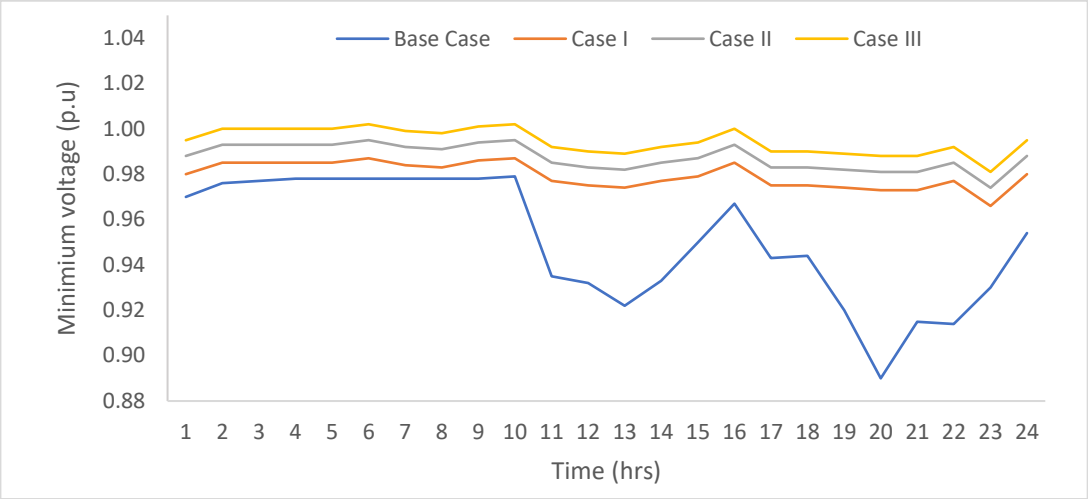

FIGURE 8: Hourly minimum bus voltage at Bus # 18 for the cases

3.1.3. Energy Loss Analysis

The daily energy loss is computed as the algebraic sum of all hourly real power losses over the day. Table 9 shows the comparison of the daily energy loss of the base case of the distribution system and after the installation of WTGs and SMES units as in cases I, II, and III.

TABLE 9: Energy loss reduction for cases I, II and III

Case	Daily energy loss		Energy loss reduction (%)
	Base case	After	
One WTG and One SMES (I)	1423.0	1005.49	29.34
Two WTGs and Two SMESs (II)	1423.0	885.68	37.76
Three WTGs and Three SMES (III)	1423.0	831.6	41.56

It is clearly observed that the energy loss reductions in the distribution system for cases I, II, and III are 29.34%, 37.76%, and 41.56%, respectively. The system's hourly power loss decreased after the installation of the WTGs and SMES units. It was also observed that after the installation of two (2) WTGs and two (2) SMES units, the energy loss decreased further by 8.4% when compared to case I, and on installing the three WTGs and three SMES units, the loss decreased by 3.8% when compared to case II. Figure 9 shows the hourly power loss of the system for the base case and cases I, II, and III.

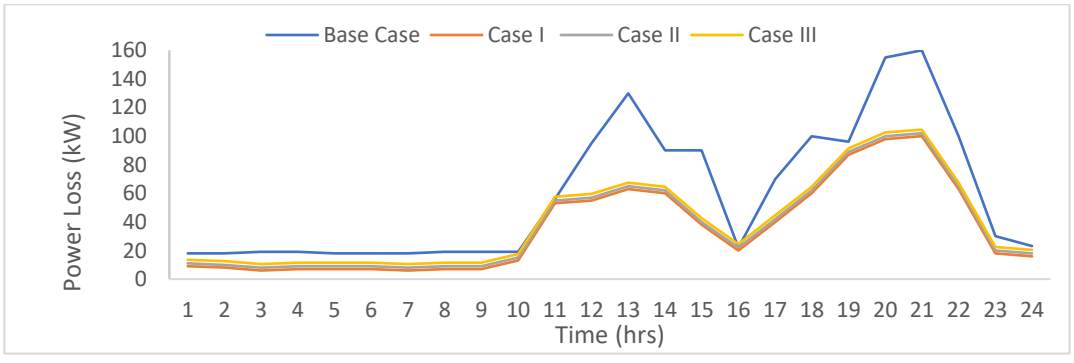

FIGURE 9: Hourly power loss for load profile

3.2. Validation of the Proposed Grasshopper Optimization Algorithm

Table 10 shows the validation of the results for the optimal location and sizing of WTGs and SMES units in the distribution system using statistical metrics and the convergence curves for each case. Figures 10, 11, and 12 show the convergence curves for each case.

TABLE 10: Statistical Metric for Case I, II and III

	CASE I			CASE II			CASE III		
Metric	GO	EO	PSO	GO	EO	PSO	GO	EO	PSO
Best	0.2679	0.4685	0.4982	0.3454	0.6437	0.8674	0.3783	0.9452	0.878
Worst	0.2568	0.4429	0.5982	0.2745	0.5277	0.7685	0.2564	0.6745	0.786
Average	0.4055	0.6334	0.6787	0.5491	0.7659	0.9459	0.6734	0.8694	0.9674
STD	0.3291	0.0173	0.1664	0.4765	0.0365	0.3245	0.5673	0.8794	0.9967
Elapse Time(s)	1648	1794	1867	2145	2254	2335	2547	27845	2985

By comparing the results of the GO algorithm with those produced using EO and PSO optimization techniques, statistical and convergence analyses are performed to assess the efficacy of the proposed EO algorithm. The statistical analysis employs various metrics to assess the effectiveness of the GO algorithm. These metrics include the best, worst, average, standard deviation (STD), and elapsed time of the multiobjective function (MOF) for all three cases. Given that the suggested GO algorithm method yields the lowest values for best, worst, average, standard deviation, and elapsed time when compared to the EO and PSO algorithms, it is evident that this approach produces the finest statistical metrics.

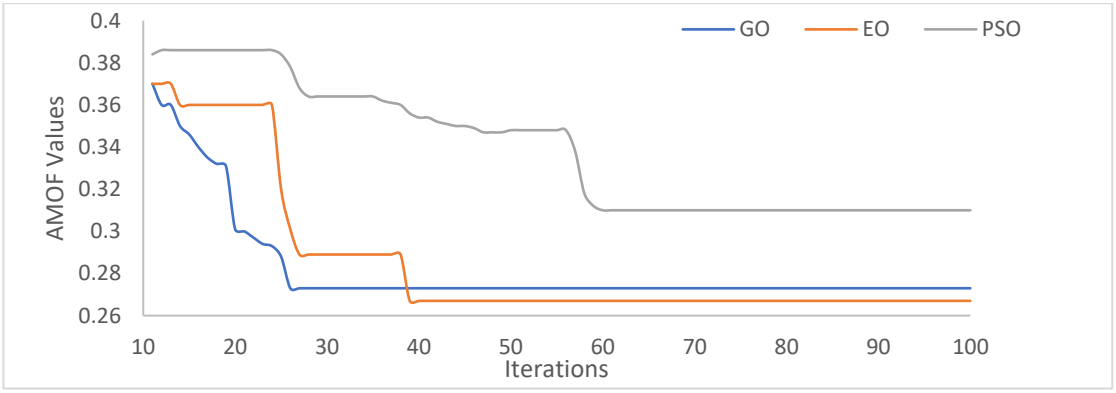

FIGURE 10: Convergence curve for case I

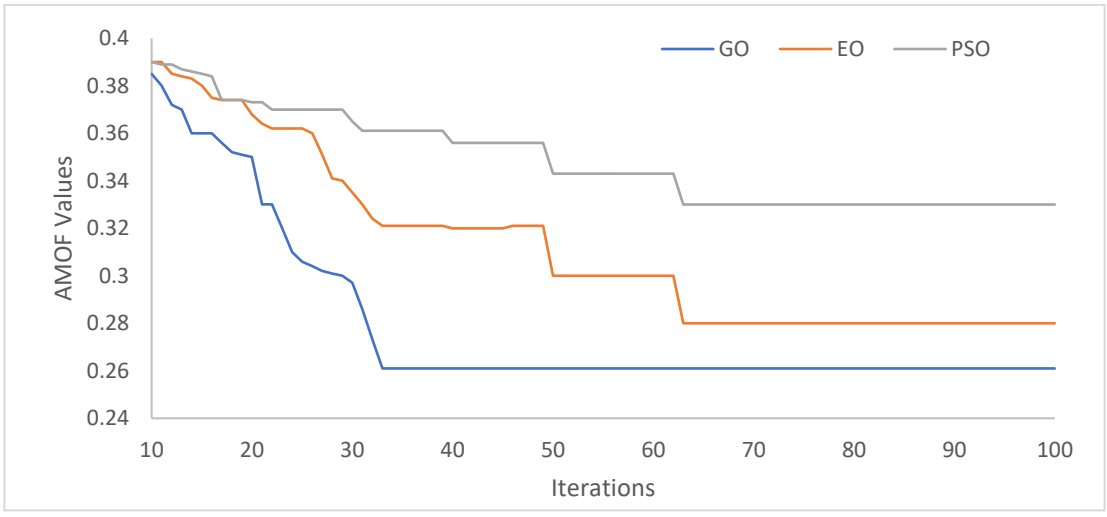

FIGURE 11: Convergence curve for case II

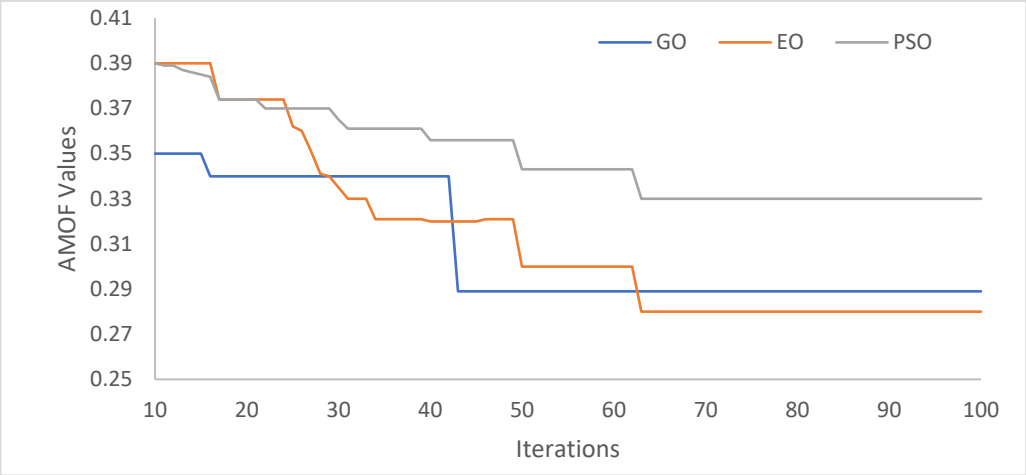

FIGURE 12: Convergence curve for case III

In convergence analysis, the comparison between convergence curves of the GO, EO, and PSO algorithms is presented for the best AMOF, as shown in Figures 10, 11, and 12 for each case study in order to demonstrate the fast convergence capability of the GO algorithm. As shown in the figures, it is clear that the proposed GO algorithm, compared with the EO and PSO algorithms, converges fast to the best AMOF after 26 seconds, 33 seconds, and 42 iterations for the respective cases.

4. Conclusion

This study presents a novel algorithm for the optimal location and sizing of WTGs and SMES units in a distribution system. The objective is to optimize the technical performance of the system while also considering the total cost. The study aimed to assess the effectiveness of the hybrid VSF and GO algorithm in determining the optimal location and size of WTGs and SMES units. This investigation considered a voltage dependent load model and the variable wind speeds. The main objectives were to improve voltage stability, minimize voltage deviation, and reduce energy loss. The findings demonstrate that the GO algorithm is a viable algorithm for improving voltage stability, reducing voltage deviation, and minimizing power loss in the IEEE 33-bus distribution system, while also considering the total cost. Additionally, it was deduced that the enhancement in voltage stability was observed, along with a reduction in voltage deviation and power loss, when the number of WTGs and SMES units were increased from one to three in each case. The effectiveness of the proposed GO algorithm was validated by comparative analysis of its statistical metrics and convergence times obtained by employing EO and PSO algorithms. The findings indicate that the GO algorithm, as described, achieves an equilibrium between exploration and exploitation, leading to a decrease in convergence time. The proposed method can be further applied to find the optimal location and size of the WTG and SMES units to improve the technical performance while considering the total cost of a larger power system in the future.

Author Contributions:

Steven Foday Sesay: Conceived, designed and performed the experiment; simulated the model, analysed the data; and wrote the paper.

Prof. Cyrus Wabuge Wekesa: Analysed the data, results, and edited the paper.

Prof. Livingstone M. H Ngoo: Analysed the data, results, and edited the paper.

Acknowledgements:

Steven Foday Sesay wishes to acknowledge African Union Commission for his scholarship.

Conflicts of Interest: None

References

[1] P. Mukherjee and V. V. Rao, "Superconducting magnetic energy storage for stabilizing grid integrated with wind power generation systems," *J. Mod. Power Syst. Clean Energy*, vol. 7, no. 2, pp. 400–411, 2019, doi: 10.1007/s40565-018-0460-y.

[2] R. Khanna, G. Singh, and T. K. Nagsarkar, "Artificial neural network based SMES unit for transient stability improvement," *2010 Jt. Int. Conf. Power Electron. Drives Energy Syst. PEDES 2010 2010 Power India*, 2010, doi: 10.1109/PEDES.2010.5712476.

[3] L. A. Wong, V. K. Ramachandaramurthy, P. Taylor, J. B. Ekanayake, S. L. Walker, and S. Padmanaban, "Review on the optimal placement, sizing and control of an energy storage system in the distribution network," *J. Energy Storage*, vol. 21, no. June 2018, pp. 489–504, 2019, doi: 10.1016/j.est.2018.12.015.

[4] M. Qolipour, A. Mostafaeipour, M. Saidi-Mehrabad, and H. R. Arabnia, "Prediction of wind speed using a new Grey-extreme learning machine hybrid algorithm: A case study," *Energy Environ.*, vol. 30, no. 1, pp. 44–62, Feb. 2019, doi: 10.1177/0958305X18787258/ASSET/IMAGE

S/LARGE/10.1177_0958305X18787258-FIG2.JPEG.

[5] R. Sadiq, Z. Wang, C. Y. Chung, C. Zhou, and C. Wang, "A review of STATCOM control for stability enhancement of power systems with wind/PV penetration: Existing research and future scope," *Int. Trans. Electr. Energy Syst.*, vol. 31, no. 11, pp. 1–27, 2021, doi: 10.1002/2050-7038.13079.

[6] A. H. Yakout, H. M. Hasanien, and H. Kotb, "Proton Exchange Membrane Fuel Cell Steady State Modeling Using Marine Predator Algorithm Optimizer," *Ain Shams Eng. J.*, vol. 12, no. 4, pp. 3765–3774, Dec. 2021, doi: 10.1016/J.ASEJ.2021.04.014.

[7] W. Buckles and W. V. Hassenzahl, "Superconducting magnetic energy storage," *IEEE Power Eng. Rev.*, vol. 20, no. 5, pp. 16–20, 2000, doi: 10.1109/39.841345.

[8] Luo, J. Wang, and C. Krupke, "Overview of Current Development in Compressed Air Energy Storage Technology," *Energy Procedia*, vol. 62, pp. 603–611, 2014, doi: 10.1016/j.egypro.2014.12.423.

[9] F. Chaychizadeh, H. Dehghandorost, A. Aliabadi, and A. Taklifi, "Stochastic dynamic simulation of a novel hybrid thermal-compressed carbon dioxide energy storage system (T-CCES) integrated with a wind farm," *Energy Convers. Manag.*, vol. 166, pp. 500–511, Jun. 2018, doi: 10.1016/J.ENCONMAN.2018.04.050.

[10] M. H. Qais, H. M. Hasanien, and S. Alghuwainem, "Output power smoothing of wind power plants using self-tuned controlled SMES units," *Electr. Power Syst. Res.*, vol. 178, no. August 2019, p. 106056, 2020, doi: 10.1016/j.epsr.2019.106056.

[11] M. H. Ali, B. Wu, and R. A. Dougal, "An overview of SMES applications in power and energy systems," *IEEE Trans. Sustain. Energy*, vol. 1, no. 1, pp. 38–47, 2010, doi: 10.1109/TSTE.2010.2044901.

[12] M. V. Aware and D. Sutanto, "Improved controller for power conditioner using high-temperature superconducting magnetic energy storage (HTS-SMES)," *IEEE Trans. Appl. Supercond.*, vol. 13, no. 1, pp. 38–47, 2003, doi: 10.1109/TASC.2003.811352.

[13] M. A. Hannan, M. M. Hoque, A. Mohamed, and A. Ayob, "Review of energy storage systems for electric vehicle applications: Issues and challenges," *Renew. Sustain. Energy Rev.*, vol. 69, pp. 771–789, Mar. 2017, doi: 10.1016/j.rser.2016.11.171.

[14] E. A. Gouda, A. Abd-Alaziz, and M. El-Saadawi, "Design modeling, and control of multi-stage SMES integrated with PV system," *J. Energy Storage*, vol. 29, p. 101399, Jun. 2020, doi: 10.1016/J.EST.2020.101399.

[15] M. C. Argyrou, P. Christodoulides, and S. A. Kalogirou, "Energy storage for electricity generation and related processes: Technologies appraisal and grid scale applications," *Renew. Sustain. Energy Rev.*, vol. 94, pp. 804–821, Oct. 2018, doi: 10.1016/J.RSER.2018.06.044.

[16] P. Mukherjee and V. V. Rao, "Design and development of high temperature superconducting magnetic energy storage for power applications - A review," *Phys. C Supercond. its Appl.*, vol. 563, pp. 67–73, Aug. 2019, doi: 10.1016/J.PHYSC.2019.05.001.

[17] İ. Aytaç, A. Sözen, K. Martin, Ç. Filiz, and H. M. Ali, "Improvement of Thermal Performance using Spineloxides/Water Nanofluids in the Heat Recovery Unit with Air-to-Air Thermosiphone Mechanism," *IJT*, vol. 41, no. 11, p. 158, Nov. 2020, doi: 10.1007/S10765-020-02739-Z.

[18] M. Ghalambaz, R. Mashayekhi, H. Arasteh, H. M. Ali, P. Talebizadehsardari, and W. Yaïci, "Thermo-Hydraulic Performance Analysis on the Effects of Truncated Twisted Tape Inserts in a Tube Heat Exchanger," *Symmetry 2020, Vol. 12, Page 1652*, vol. 12, no. 10, p. 1652, Oct. 2020, doi: 10.3390/SYM12101652.

[19] X. Wang *et al.*, "Vegetable oil-based nanofluid minimum quantity lubrication turning: Academic review and perspectives," *J. Manuf. Process.*, vol. 59, pp. 76–97, Nov. 2020, doi: 10.1016/J.JMAPRO.2020.09.044.

[20] U. Sajjad, A. Sadeghianjahromi, H. M. Ali, and C. C. Wang, "Enhanced pool boiling of dielectric and highly wetting liquids - a review on enhancement mechanisms," *Int. Commun. Heat Mass Transf.*, vol. 119, p. 104950, Dec. 2020, doi: 10.1016/J.ICHEATMASSTRANSFER.2020.104950.

[21] A. Shahsavar, S. S. Alimohammadi, I. B. Askari, and H. M. Ali, "Numerical investigation of the effect of corrugation profile on the hydrothermal characteristics and entropy generation behavior of laminar forced convection of non-Newtonian water/CMC-CuO nanofluid flow inside a wavy channel," *Int. Commun. Heat Mass Transf.*, vol. 121, p. 105117, Feb. 2021, doi: 10.1016/J.ICHEATMASSTRANSFER.2021.105117.

[22] H. M. Ali, "Recent advancements in PV cooling and efficiency enhancement integrating phase change materials based systems – A comprehensive review," *Sol. Energy*, vol. 197, pp. 163–198, Feb. 2020, doi: 10.1016/J.SOLENER.2019.11.075.

[23] H. M. Hasanien and S. M. Muyeen, "Particle swarm optimization-based superconducting magnetic energy storage for low-voltage ride-through capability enhancement in wind energy conversion system," *Electr. Power Components Syst.*, vol. 43, no. 11, pp. 1278–

1288, Jul. 2015, doi: 10.1080/15325008.2015.1027017.

[24] H. M. Hasanien, S. Q. Ali, and S. M. Muyeen, "Wind generator stability enhancement by using an adaptive artificial neural network-controlled superconducting magnetic energy storage," *ICEMS 2012 - Proc. 15th Int. Conf. Electr. Mach. Syst.*, no. August 2017, 2012.

[25] S. M. Said and B. Hartmann, "Alleviation of Extremely Power and Voltage Variations Caused by Wind Power and Load Demand Using SMES," vol. 63, no. 3, pp. 134–143, 2019.

[26] M. H. Ali, T. Murata, and J. Tamura, "Transient stability enhancement by fuzzy logic-controlled SMES considering coordination with optimal reclosing of circuit breakers," *IEEE Trans. Power Syst.*, vol. 23, no. 2, pp. 631–640, May 2008, doi: 10.1109/TPWRS.2008.920045.

[27] W. Kreeumporn and I. Ngamroo, "Optimal Superconducting Coil Integrated into PV Generators for Smoothing Power and Regulating Voltage in Distribution System with PHEVs," *IEEE Trans. Appl. Supercond.*, vol. 26, no. 7, 2016, doi: 10.1109/TASC.2016.2591981.

[28] T. Chaiyatham and I. Ngamroo, "OPTIMAL FUZZY GAIN SCHEDULING OF PID CONTROLLER OF SUPERCONDUCTING MAGNETIC ENERGY STORAGE FOR POWER SYSTEM STABILIZATION," *Int. J. Innov. Comput. Inf. Control ICIC Int. c*, vol. 9, no. 2, pp. 651–666, 2013.

[29] A. Boudia, S. Messalti, A. Harrag, and M. Boukhnifer, "New hybrid photovoltaic system connected to superconducting magnetic energy storage controlled by PID-fuzzy controller," *Energy Convers. Manag.*, vol. 244, no. February, p. 114435, 2021, doi: 10.1016/j.enconman.2021.114435.

[30] X. Jiang *et al.*, "SMES system for study on utility and customer power applications," *IEEE Trans. Appl. Supercond.*, vol. 11, no. 1 II, pp. 1765–1769, Mar. 2001, doi: 10.1109/77.920126.

[31] B. K. Kang, S. T. Kim, B. C. Sung, and J. W. Park, "A study on optimal sizing of superconducting magnetic energy storage in distribution power system," *IEEE Trans. Appl. Supercond.*, vol. 22, no. 3, 2012, doi: 10.1109/TASC.2011.2174571.

[32] S. J. Lee, "Location of a superconducting device in a power grid for system loss minimization using loss sensitivity," *IEEE Trans. Appl. Supercond.*, vol. 17, no. 2, pp. 2351–2354, 2007, doi: 10.1109/TASC.2007.898435.

[33] S. Saranya and B. Saravanan, "Optimal size allocation of superconducting magnetic energy storage system based unit commitment," *J. Energy Storage*, vol. 20, no. September, pp. 173–189, 2018, doi: 10.1016/j.est.2018.09.011.

[34] M. Hashem, M. Abdel-Salam, M. T. El-Mohandes, M. Nayel, and M. Ebeed, "Optimal Placement and Sizing of Wind Turbine Generators and Superconducting Magnetic Energy Storages in a Distribution System," *J. Energy Storage*, vol. 38, no. March, p. 102497, 2021, doi: 10.1016/j.est.2021.102497.

[35] D. Quoc Hung, S. Member, N. Mithulananthan, S. Member, and K. Y. Lee, "Determining PV Penetration for Distribution Systems With Time-Varying Load Models," 2014, doi: 10.1109/TPWRS.2014.2314133.

[36] O. Khoubseresht and H. Shayanfar, "The role of demand response in optimal sizing and siting of distribution energy resources in distribution network with time-varying load: An analytical approach," *Electr. Power Syst. Res.*, vol. 180, p. 106100, Mar. 2020, doi: 10.1016/J.EPSR.2019.106100.

[37] E. E. Sfikas, Y. A. Katsigiannis, and P. S. Georgilakis, "Simultaneous capacity optimization of distributed generation and storage in medium voltage microgrids," *Int. J. Electr. Power Energy Syst.*, vol. 67, pp. 101–113, May 2015, doi: 10.1016/J.IJEPES.2014.11.009.

[38] M. A. Mohamed, A. M. Eltamaly, A. I. Alolah, and A. Y. Hatata, "A novel framework-based cuckoo search algorithm for sizing and optimization of grid-independent hybrid renewable energy systems," *Int. J. Green Energy*, vol. 16, no. 1, pp. 86–100, 2019, doi: 10.1080/15435075.2018.1533837.

[39] D. Q. Hung, N. Mithulananthan, and R. C. Bansal, "Analytical strategies for renewable distributed generation integration considering energy loss minimization," *Appl. Energy*, vol. 105, pp. 75–85, 2013, doi: 10.1016/j.apenergy.2012.12.023.

[40] P. Mukherjee and V. V. Rao, "Design and development of high temperature superconducting magnetic energy storage for power applications - A review," *undefined*, vol. 563, pp. 67–73, Aug. 2019, doi: 10.1016/J.PHYSC.2019.05.001.

[41] Z. Chen, X. Y. Xiao, C. S. Li, Y. Zhang, and Z. X. Zheng, "Study on Unit Commitment Problem Considering Large-Scale Superconducting Magnetic Energy Storage Systems," *IEEE Trans. Appl. Supercond.*, vol. 26, no. 7, Oct. 2016, doi: 10.1109/TASC.2016.2598353.

[42] L. F. Montoya, Q. Fu, A. Nasiri, V. Bhavaraju, and D. Yu, "Novel methodology to determine the optimal energy storage location in a microgrid and address power quality and stability," *White Pap. WP083008EN*, no. May, 2014, [Online]. Available: www.eaton.com.

[43] E. S. Ali, S. M. Abd Elazim, and A. Y. Abdelaziz, "Ant Lion Optimization Algorithm for optimal location and sizing of renewable distributed generations," *Renew. Energy*, vol. 101, pp. 1311–1324, 2017, doi: 10.1016/j.renene.2016.09.023.

[44] A. S. Hassan, E. S. A. Othman, F. M. Bendary, and M. A. Ebrahim, "Improving the Techno-Economic Pattern for Distributed Generation-

Based Distribution Networks via Nature-Inspired Optimization Algorithms," *Technol. Econ. Smart Grids Sustain. Energy*, vol. 7, no. 1, 2022, doi: 10.1007/s40866-022-00128-z.

[45] B. Ahmadi, O. Ceylan, and A. Ozdemir, "Distributed energy resource allocation using multi-objective grasshopper optimization algorithm," *Electr. Power Syst. Res.*, vol. 201, no. December 2020, p. 107564, 2021, doi: 10.1016/j.epsr.2021.107564.

[46] A. Gayathri, V. Rukkumani, V. Manimegalai, and P. Pandiyan, "A Comprehensive Review on Energy Storage Systems," *Smart Electr. Grid Syst.*, pp. 211–251, 2022, doi: 10.1201/9781003242277-15.

[47] A. D. Petropoulos, N. C. Koutsoukis, E. S. Karapidakis, and P. S. Georgilakis, "Optimal mix of wind generation and energy storage systems in power distribution networks," *IET Conf. Publ.*, vol. 2014, no. CP665, 2014, doi: 10.1049/CP.2014.1640.

[48] D. Sutanto and K. W. E. Cheng, "Superconducting magnetic energy storage systems for power system applications," *2009 Int. Conf. Appl. Supercond. Electromagn. Devices, ASEMD 2009*, pp. 377–380, 2009, doi: 10.1109/ASEMD.2009.5306614.

[49] M. N. Kiio, C. W. Wekesa, and S. I. Kamau, "Evaluating Performance of a Linear Hybrid State Estimator Utilizing Measurements from RTUs and Optimally Placed PMUs," *IEEE Access*, vol. 10, pp. 63113–63131, 2022, doi: 10.1109/ACCESS.2022.3182338.

[50] D. H. Wolpert and W. G. Macready, "No free lunch theorems for optimization," *IEEE Trans. Evol. Comput.*, vol. 1, no. 1, pp. 67–82, 1997, doi: 10.1109/4235.585893.

[51] S. Saremi, S. Mirjalili, and A. Lewis, "Grasshopper Optimisation Algorithm: Theory and application," *Adv. Eng. Softw.*, vol. 105, pp. 30–47, 2017, doi: 10.1016/j.advengsoft.2017.01.004.

[52] A. Hatata and S. Kaddah, "Grasshopper Optimization-based Optimal Sizing of DG/DSTATCOM in Distribution Networks," no. May, 2022, doi: 10.21608/bfemu.2022.238659.

[53] P. P. Kumar, R. S. S. Nuvvula, and V. Manoj, "Grass Hopper Optimization Algorithm for Off-Grid Rural Electrification of an Integrated Renewable Energy System," *E3S Web Conf.*, vol. 350, p. 02008, 2022, doi: 10.1051/e3sconf/202235002008.